A&A, 706, A239 (2026)
https://doi.org/10.1051/0004-6361/202557670

Astronomy & Astrophysics

Violent mergers revisited: The origin of the fastest stars in the Galaxy

Rüdiger Pakmor[1,⋆], Ken J. Shen[2], Aakash Bhat[3], Abinaya Swaruba Rajamuthukumar[1], Christine E. Collins[4], Cillian O'Donnell[4], Evan B. Bauer[5,6], Fionntan P. Callan[7], Friedrich K. Röpke[8,9,10], Joshua M. Pollin[7], Kate Maguire[4], Lindsey A. Kwok[11], Ravi Seth[4], Stefan Taubenberger[12,1], and Stephen Justham[1]

[1] Max-Planck-Institut für Astrophysik, Karl-Schwarzschild-Str. 1, D-85748 Garching, Germany
[2] Department of Astronomy and Theoretical Astrophysics Center, University of California, Berkeley, CA 94720-3411, USA
[3] Institut für Physik und Astronomie, Universität Potsdam, Haus 28, Karl-Liebknecht-Str. 24/25, 14476 Potsdam-Golm, Germany
[4] School of Physics, Trinity College Dublin, College Green, Dublin 2, Ireland
[5] Lawrence Livermore National Laboratory, Livermore, California 94550, USA
[6] Center for Astrophysics | Harvard & Smithsonian, 60 Garden Street, Cambridge, MA 02138, USA
[7] School of Mathematics and Physics, Queen's University Belfast, University Road, Belfast BT7 1NN, UK
[8] Zentrum für Astronomie der Universität Heidelberg, Astronomisches Recheninstitut, Mönchhofstrasse 12–14, 69120 Heidelberg, Germany
[9] Heidelberger Institut für Theoretische Studien, Schloss-Wolfsbrunnenweg 35, 69118 Heidelberg, Germany
[10] Zentrum für Astronomie der Universität Heidelberg, Institut für Theoretische Astrophysik, Philosophenweg 12, 69120 Heidelberg, Germany
[11] Center for Interdisciplinary Exploration and Research in Astrophysics (CIERA), 1800 Sherman Ave., Evanston, IL 60201, USA
[12] TUM Department of Physics, Technical University Munich, Garching, Germany

Received 13 October 2025 / Accepted 29 December 2025

ABSTRACT

Binary systems of two carbon-oxygen white dwarfs are one of the most promising candidates for the progenitor systems of Type Ia supernovae. Violent mergers, where the primary white dwarf ignites when the secondary white dwarf smashes into it while being disrupted on its last orbit, were the first double degenerate merger scenario proposed that ignites dynamically. However, violent mergers likely contribute only a few percent to the total Type Ia supernova rate and do not yield normal Type Ia supernova light curves. Here we revisit the scenario, simulating a violent merger with better methods and, in particular, a more accurate treatment of the detonation. We find good agreement with previous simulations but with one critical difference: The secondary white dwarf being disrupted and accelerated towards the primary white dwarf and impacted by its explosion does not fully burn, and its core survives as a bound object. The explosion leaves behind a $0.16\,M_\odot$ star travelling 2800 km/s, making it an excellent (and so far the only) candidate to explain the origin of the fastest observed hypervelocity stars. We also show that before the explosion, $5 \times 10^{-3}\,M_\odot$ of material predominantly consisting of helium, carbon, and oxygen had already been ejected at velocities above 1000 km/s. Finally, we argue that if a violent merger made the hypervelocity stars D6-1 and D6-3 and violent mergers require the most massive primary white dwarfs in binaries of two carbon-oxygen white dwarfs, there has to be a much larger population of white dwarf mergers with slightly lower mass primary white dwarfs. Because this population likely represents $\gg$10% of the Type Ia supernovae rate, it can essentially only give rise to normal Type Ia supernovae.

Key words. hydrodynamics – nuclear reactions, nucleosynthesis, abundances – methods: numerical – binaries: general – supernovae: general

1. Introduction

The progenitor systems and explosion mechanism of Type Ia supernovae are still debated. A general consensus has only been achieved on the concept that they are thermonuclear explosions of carbon-oxygen white dwarfs in binary systems (Liu et al. 2023; Ruiter & Seitenzahl 2025).

Mergers of two carbon-oxygen white dwarfs in a binary system have long been studied as one potential progenitor channel. However, the originally proposed 'slow' merger channel in which the binary merges into a rotationally supported object that surpasses the Chandrasekhar mass and eventually contracts and explodes has been consistently shown not to work. It instead seems to lead to an accretion induced collapse to a neutron star (Saio & Nomoto 1985; Shen et al. 2012; Schwab et al. 2012; Schwab 2021).

Nevertheless, as first shown in Pakmor et al. (2010), the binary system might already explode dynamically during the actual merger, as a 'violent merger' explosion (Pakmor et al. 2010, 2011, 2012a; Sato et al. 2015, 2016). In this scenario, when the secondary white dwarf is disrupted on its last orbit and accelerated towards the primary white dwarf, its impact on the surface of the primary white dwarf directly ignites a carbon detonation there. This detonation then sweeps through the primary white dwarf and the remains of the secondary white dwarf, and the explosion fully unbinds the system (Pakmor et al. 2010, 2012a; Sato et al. 2015). Initially proposed as a channel to produce normal Type Ia supernovae, because it matches various early time observables reasonably well (Pakmor et al. 2012a), violent mergers were soon shown to likely only produce peculiar explosions that fade more slowly and are more asymmetric than normal Type Ia supernovae (Kromer et al. 2013a; Bulla et al. 2016).

⋆ Corresponding author: rpakmor@mpa-garching.mpg.de

Shortly after the violent merger scenario was proposed, it was realised that the helium shell inherent to the surface of any carbon-oxygen white dwarf likely facilitates an explosion of at least the primary white dwarf of the binary via the double detonation mechanism long before the system actually merges (Guillochon et al. 2010; Pakmor et al. 2013; Shen & Moore 2014). This scenario will likely work for most systems that have a massive enough helium shell on the primary white dwarf, and it only fails for the most massive primary white dwarfs, which have the smallest helium shells (Shen et al. 2024). Thus, the violent merger channel fell out of focus.

Later, the violent merger scenario was shown to explain many aspects of some peculiar Type Ia supernovae well. The over-luminous Type Ia supernova sub-class of '03fg-like' events have been connected to violent mergers where the extra luminosity compared to a normal Type Ia supernova is explained by interaction with the material of the disrupted secondary white dwarf (Dimitriadis et al. 2022; Siebert et al. 2023, 2024; Kwok et al. 2024). They have also been suggested to explain the broad light curves and sub-luminous nature of the Type Ia supernova sub-class of '02es-like' events (Maguire et al. 2011; Ganeshalingam et al. 2012; Kromer et al. 2013a; Srivastav et al. 2023a). Both of these classes have been observationally shown to have flux excesses ('bumps') in their early light curves that are absent for other Type Ia supernova classes, pointing to a unifying explosion scenario (Hoogendam et al. 2024), which has been argued to be the violent merger model.

Here, we revisit the violent merger scenario, simulating the explosion of a binary system consisting of two $1.1\,M_\odot$ and $0.7\,M_\odot$ carbon-oxygen white dwarfs with the moving mesh code AREPO (Springel 2010; Pakmor et al. 2016; Weinberger et al. 2020). Notably, in this work we are able to follow the pre-merger evolution more faithfully and at better numerical resolution than previous simulations. Moreover, we model the nuclear burning in the detonation more accurately than the original simulations (Pakmor et al. 2012b).

We summarise the methods and setup of our simulation in Sect. 2. We then show in Sect. 3 that the inspiral, ignition, and explosion are in many aspects very similar to previous simulations of violent mergers. However, we find one critical difference: The secondary white dwarf is not fully burned. Despite being partially disrupted at the time of ignition and hit by the explosion, its core survives the explosion and remains bound. We characterise the bound remnant in Sect. 4 and argue that this surviving very low mass and fast moving star is a good candidate to explain the extreme hypervelocity stars D6-1 and D6-3 found with *Gaia* (Shen et al. 2018).

Our new simulation models the initial inspiral for an unprecedented length of time. We exploit this to analyse the properties of the material that is expelled from the binary system during the last phase of the inspiral to form circumstellar material in Sect. 5. We discuss the impact of our results for violent mergers, and in general for peculiar supernovae and normal Type Ia supernovae in Sect. 6. Finally, we conclude with a summary and a description of our outlook in Sect. 7.

2. Methods

Our simulation setup consists of three distinct steps. Using the stellar evolution code MESA (Paxton et al. 2011), we first generated white dwarfs with the desired masses and a realistic composition profile by evolving helium-burning stars in isolation until they cease burning and cool as white dwarfs. Here, we follow the recipe used and described in detail in Shen et al. (2023).

We then generated isolated 3D white dwarfs with the same radial profiles in the moving mesh magnetohydrodynamics code AREPO (Springel 2010; Pakmor et al. 2016; Weinberger et al. 2020), which we used to simulate the inspiral and explosion in a similar setup as other recent white dwarf merger simulations with AREPO (Pakmor et al. 2021, 2022; Burmester et al. 2023; Glanz et al. 2025). AREPO implements a second-order finite-volume scheme for magnetohydrodynamics on a moving Voronoi mesh. The mesh is evolved in an approximately Lagrangian way, that is, a set of mesh-generating points that move with the local gas velocity with small corrections to keep the mesh regular. Self-gravity is computed with the oct-tree method (Springel 2005).

We employed explicit refinement and de-refinement of cells that deviate more than a factor of two from the target gas mass of $10^{-7}\,M_\odot$. Additionally, we used a passive tracer to mark the helium shells on both white dwarfs to resolve them at a ten times better mass resolution of $10^{-8}\,M_\odot$. This allowed us to even resolve helium shells below $10^{-3}\,M_\odot$.

We used the Helmholtz equation of state (Timmes & Swesty 2000) that models an arbitrarily degenerate electron-positron gas, as well as ions, as fully ionised non-degenerate ideal gas with additional Coulomb corrections, and includes radiation. We also fully couple a 55 isotope nuclear reaction network (Pakmor et al. 2012a, 2021) with JINA reaction rates (Cyburt et al. 2010). The nuclear reaction network is active for all cells with a temperature $T > 10^6\,\mathrm{K}$. We use a standard burning limiter to disable nuclear burning in shocks to ensure that the unresolved detonation propagates at the correct speed (Fryxell et al. 1989; Seitenzahl et al. 2009; Pakmor et al. 2021).

To map the white dwarfs from MESA to AREPO, we first generated approximate 3D representations of the 1D density profiles of the white dwarfs with roughly round cells of approximately equal mass using HEALPix tessellations of spherical surfaces (Pakmor et al. 2012a; Ohlmann et al. 2017). We then mapped the precise density and composition profile of the white dwarfs and evolved them for ten sound-crossing timescales. We relaxed them with a time-dependent friction term for the first five sound-crossing times, and then we evolved them freely for another five sound-crossing times to make sure they are stable.

3. Inspiral and explosion

Our initial binary system consists of a primary white dwarf with a total mass of $1.1\,M_\odot$ and a secondary white dwarf with a total mass of $0.7\,M_\odot$. The primary white dwarf comes out to consist of essentially equal amounts of $0.54\,M_\odot$ each of carbon and oxygen, mixed with $0.016\,M_\odot$ of ^{22}Ne, and a helium shell of $3 \times 10^{-4}\,M_\odot$. It has a radius of 4600 km, and its helium shell, defined as range in which the helium mass fraction is larger than 0.1, has a width of 200 km. The secondary white dwarf is made of $0.32\,M_\odot$ of carbon, $0.36\,M_\odot$ of oxygen, $0.011\,M_\odot$ of ^{22}Ne, and a helium shell of $0.009\,M_\odot$. It has a radius of 7600 km and a helium shell with a width of 1100 km.

After having relaxed both white dwarfs separately, we put them together in a binary system in co-rotation with an initial separation of 3.2×10^9 cm, equivalent to an initial orbital period of 74 s. At this distance, the secondary white dwarf does not fill its Roche lobe. The inspiral then proceeds in three steps. We show the full evolution of the binary separation with time in Fig. 1.

In the first phase, we apply an artificial gravitational wave-like source term that removes angular momentum and shrinks the binary separation at a constant rate (Pakmor et al. 2021, 2022). In this phase we shrink the binary system at a rate of

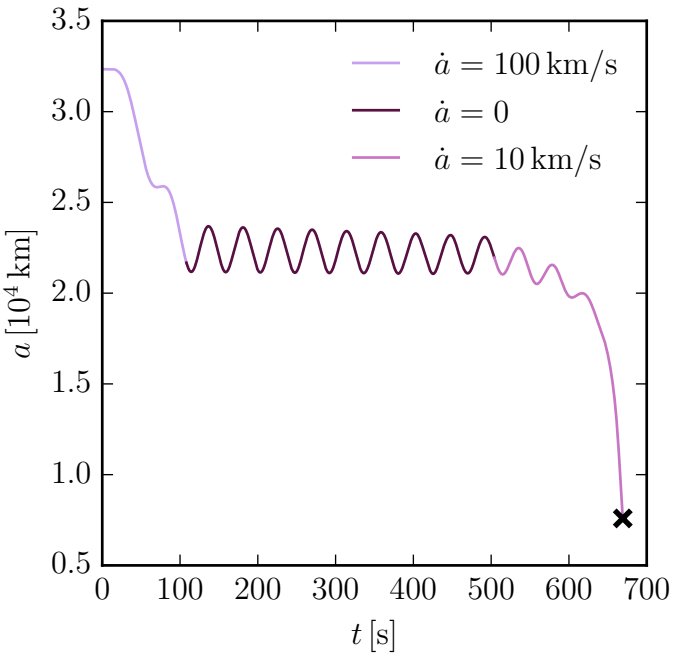

Fig. 1. Time evolution of the separation between the two white dwarfs computed as the distance between the centres of mass of the material originating from both white dwarfs. We first shrank the binary system at a constant rate of 100 km/s for 108 s. We then evolved it for another 395 s self-consistently (i.e. the total angular momentum in the simulation was conserved). In this phase, mass transfer only shrinks it at a rate of ≈0.5 km/s. We then actively shrank it again at a rate of 10 km/s until it merged 166 s later. The cross denotes the time of explosion.

$\dot{a} = 100\,\mathrm{km/s}$ for 108 s, until it reaches a separation of 2.2×10^9 cm, equivalent to an orbital period of 41 s. At this time the density at the inner Lagrange point L1 reaches $10^4\,\mathrm{g\,cm^{-3}}$ (which is typically sufficient to quickly lead to helium ignition on the primary white dwarf if there is sufficient helium on it; see for example Pakmor et al. 2022). Note that the small eccentricity during this phase is a result of the relatively fast initial inspiral. To avoid this, we likely have to ensure that the distance only changes by a small amount in every orbit, that is $\dot{a} \ll a/P \approx 500\,\mathrm{km/s}$, where P is the orbital period. However, we currently cannot afford the computational cost to evolve the system this slowly all the way from the time the secondary white dwarf fills its Roche-lobe to the explosion.

In the second phase, we then continue to evolve the binary system for 395 s without the artificial angular momentum loss term, that is, we conserve the total angular momentum of the system. In this phase, the binary separation continues to shrink as a result of mass transfer, but only at a very small rate of $\dot{a} \lesssim 0.5\,\mathrm{km/s}$, barely visible in Fig. 1.

Realising that computational limitations would not allow us to evolve the system to the point where it merges this way, we enabled the angular momentum loss term again in the third phase. In this phase, we actively shrank the system again at a constant rate, but we reduced it to a tenth of the initial rate, that is, to $\dot{a} = 10\,\mathrm{km/s}$, which is still 20 times faster than the physical rate. We kept this term active until the system merged and plausibly ignites 166 s later. Having the angular momentum loss term active until the system explodes might affect the detailed properties of the material ejected prior to the merger and of the secondary white dwarf during the merger. This is mostly limited by computational constraints and should be investigated in more detail in the future.

At the time of ignition, the total angular momentum of the binary system, that is the total angular momentum of all material in our simulation relative to the centre and in the rest frame of the binary system, had decreased to $6.3 \times 10^{50}\,\mathrm{g\,cm^2\,s^{-1}}$ from $6.5 \times 10^{50}\,\mathrm{g\,cm^2\,s^{-1}}$ during the intermediate phase that conserved angular momentum. During the second and third inspiral phases, all the helium initially present on the surface of the secondary white dwarf was transferred to the primary white dwarf. Of this helium, $5 \times 10^{-3}\,M_\odot$ was burned in bursts on the surface of the primary white dwarf. This ejected the ashes of the helium burning as well as the remaining unburned helium from the system (see also Sect. 5). In contrast to previous simulations with more massive helium shells on the primary white dwarf (for example Pakmor et al. 2013, 2022), the helium shell on our $1.1\,\mathrm{M_\odot}$ primary white dwarf is too small to sustain a helium detonation (Shen et al. 2024). Therefore, there is also no core ignition via the double detonation scenario.

At 668 s, the secondary white dwarf is being disrupted and accelerated towards the primary. As it hits the primary white dwarf directly, material on the surface of the primary white dwarf is compressed and heated up to reach conditions favourable for carbon ignition, similar to previous violent merger simulations (Pakmor et al. 2010, 2012a; Sato et al. 2015). Figure 2 shows slices of density and temperature of the binary system in the plane of rotation at the time of ignition. The centres of mass of the material originating from both white dwarfs are denoted by black crosses. The centre of mass of the material originating from the secondary white dwarf directly show that it is already quite advanced in the process of being disrupted, as its centre is significantly offset from where the density peak in its tail. The purple circle shows the spot that contains 32 cells with a density larger than $\rho = 2 \times 10^6\,\mathrm{g\,cm^{-3}}$ as well as a temperature above $T = 10^9$ K. It provides plausible conditions to ignite a carbon detonation (Seitenzahl et al. 2009).

The ignition is not resolved by many orders of magnitude in spatial scale, so we put in a detonation at this spot by heating all material within a sphere of radius 100 km to a temperature of 5×10^9 K. This injects a total energy of 4.8×10^{46} erg into 188 cells with a total mass of $5 \times 10^{-6}\,\mathrm{M_\odot}$ and starts a detonation. The detonation burns through the primary white dwarf and releases 1.7×10^{51} erg of nuclear energy. The explosion destroys the primary white dwarf. Its ejecta impact the secondary white dwarf that is already in a state of being disrupted, and unbind most of it as well. In contrast to previous violent merger simulations (Pakmor et al. 2010, 2012a), the secondary white dwarf is not fully burned. Rather, a small fraction ($0.16\,M_\odot$) of its core remains bound and even accretes a small amount of the ashes of the primary white dwarf on its surface. The location of the material that will make up the bound remnant is indicated with black contours in the left panel of Fig. 2. Almost all of the material that will make up the bound remnant is contained in the upper contour that only contains material that originates from the secondary white dwarf. The lower contour that marks material which originates from the primary white dwarf only contributes $0.002\,\mathrm{M_\odot}$ to the bound remnant, or roughly 1% of its mass. Thus, only a tiny fraction of the mass covered by the lower contour will become part of the bound remnant. We will discuss the properties of this remnant in detail in Sect. 4.

The main difference to previous violent merger models of a similar system (Pakmor et al. 2012a) is that they used the level-set method to model the detonation. That method models the detonation as a shock discontinuity that propagates with a given velocity and instantaneously burns material that is crossed by the detonation. It assumes that the composition of the material

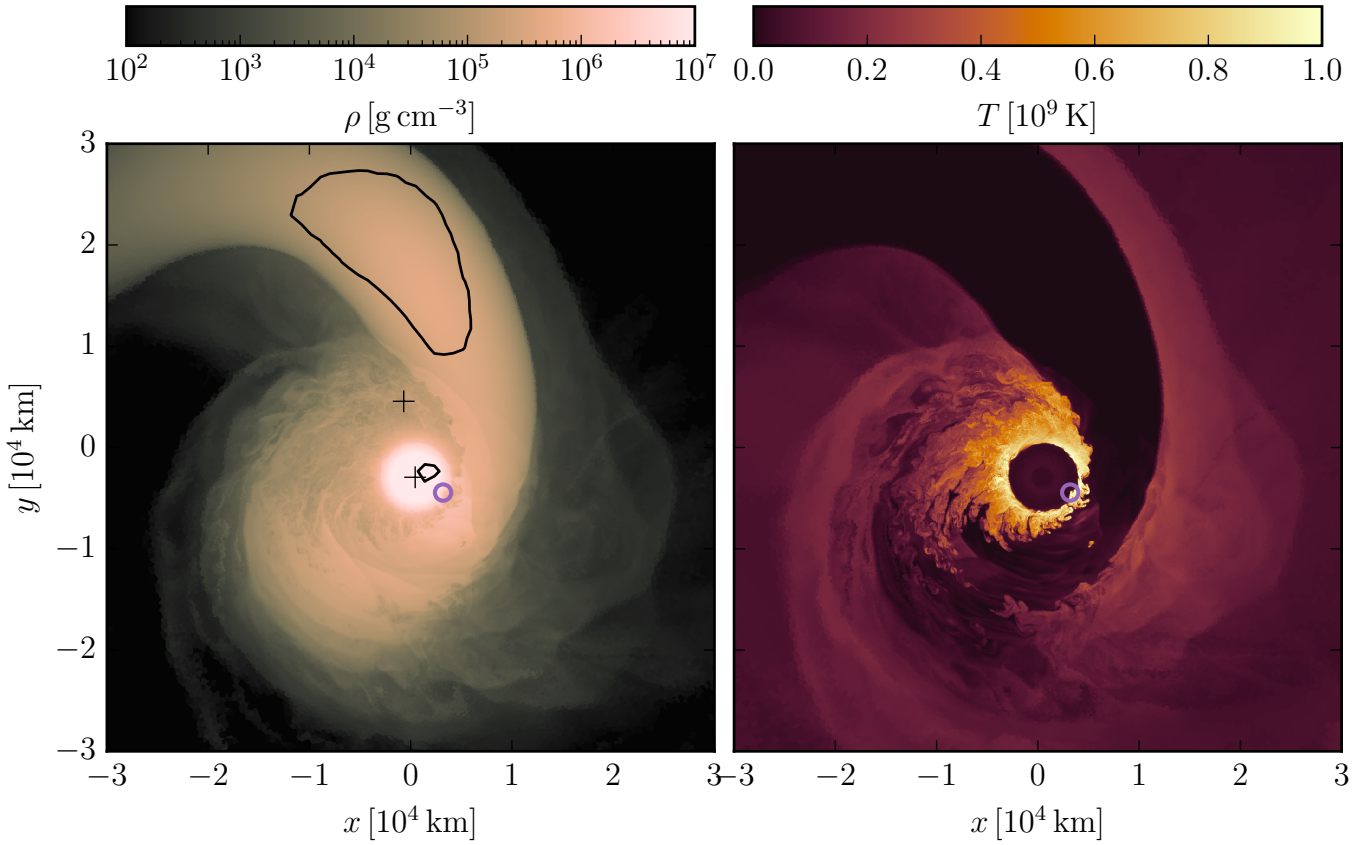

Fig. 2. Density (left panel) and temperature (right panel) slices of the binary system during the merger at the time when it reaches conditions for carbon ignition. The purple circle shows the point where 32 cells reach a temperature of 10^9 K at a density of 2×10^6 g cm^{-3}. We ignited a detonation there (see text). The contours in the left panel show the origin of 95% of the material that will become the bound remnant after the explosion. The crosses in the left panel show the centres of mass of the material originating from each white dwarf.

after it has been burned only depends on the pre-shock density, which is tabulated. However, this approximation ignores that the burning also depends on the strength of the shock, which can change as the shock propagates. A stronger shock compresses the material more before it is burned, and the nuclear burning proceeds further. The nuclear burning with the level-set method is typically calibrated to a centrally ignited spherical white dwarf. In this setup the shock travels down the density gradient and becomes stronger with time. Critically, a specific shock strength at each density is implicitly baked into this calibration. Because the detonation starts at the densest point, this setup for calibration likely leads to the strongest possible detonation shock and therefore the farthest nuclear burning.

In our simulation, in contrast, the detonation is directly modelled by solving the full time-dependent reactive Euler equations. That is, in every time step a nuclear reaction network is fully coupled to the equations of hydrodynamics. The composition of each cell changes following the time integration of the nuclear reaction rates, and the nuclear energy release directly changes the internal energy of the cell.

Despite not resolving the physical width of the carbon detonation by many orders of magnitude, this method in principle reproduces the change of composition and energy release from nuclear burning from the detonation on the scales we resolved (Fryxell et al. 1989; Seitenzahl et al. 2009; Pakmor et al. 2013; Kushnir & Katz 2020). One caveat is that because we do not resolve the physical width of the detonation shock, we needed to limit nuclear burning in the shock itself (Fryxell et al. 1989). Here, we configured the limiter so that it would more aggressively label pressure jumps as shocks (Pakmor et al. 2021), which usually leads to the furthest burning and largest energy release compared to milder limiters.

In our simulation the explosion of the primary white dwarfs launches a strong shock towards the secondary white dwarf. This shock is strongest when it just hits the secondary white dwarf that is already being disrupted. At this time, the central density of the secondary white dwarf has already dropped below 5×10^5 g cm^{-3}. The shock burns some of the carbon in the outer layers of the secondary white dwarf to neon and heavier intermediate mass elements. However, the shock weakens as it travels up the density gradient and the energy release from nuclear burning is insufficient to sustain the strength of the shock at these densities (Dunkley et al. 2013). Nuclear burning then essentially ceases in the core of the secondary white dwarf, and a fraction of the core remains bound and unburned. Note that because of our aggressive burning limiter, it is unlikely that a different treatment of the unresolved detonation in AREPO would burn the whole secondary white dwarf.

Similar to previous violent merger simulations the ejecta of the primary expand much more easily in the vertical direction compared to the plane of rotation, where they encounter the material of the partially disrupted secondary white dwarf. This also implies that the impact of the ejecta of the primary white dwarf on the secondary white dwarf is weaker compared to isotropic expansion of the ejecta of the primary white dwarf. The material that is unbound from the secondary from the impact

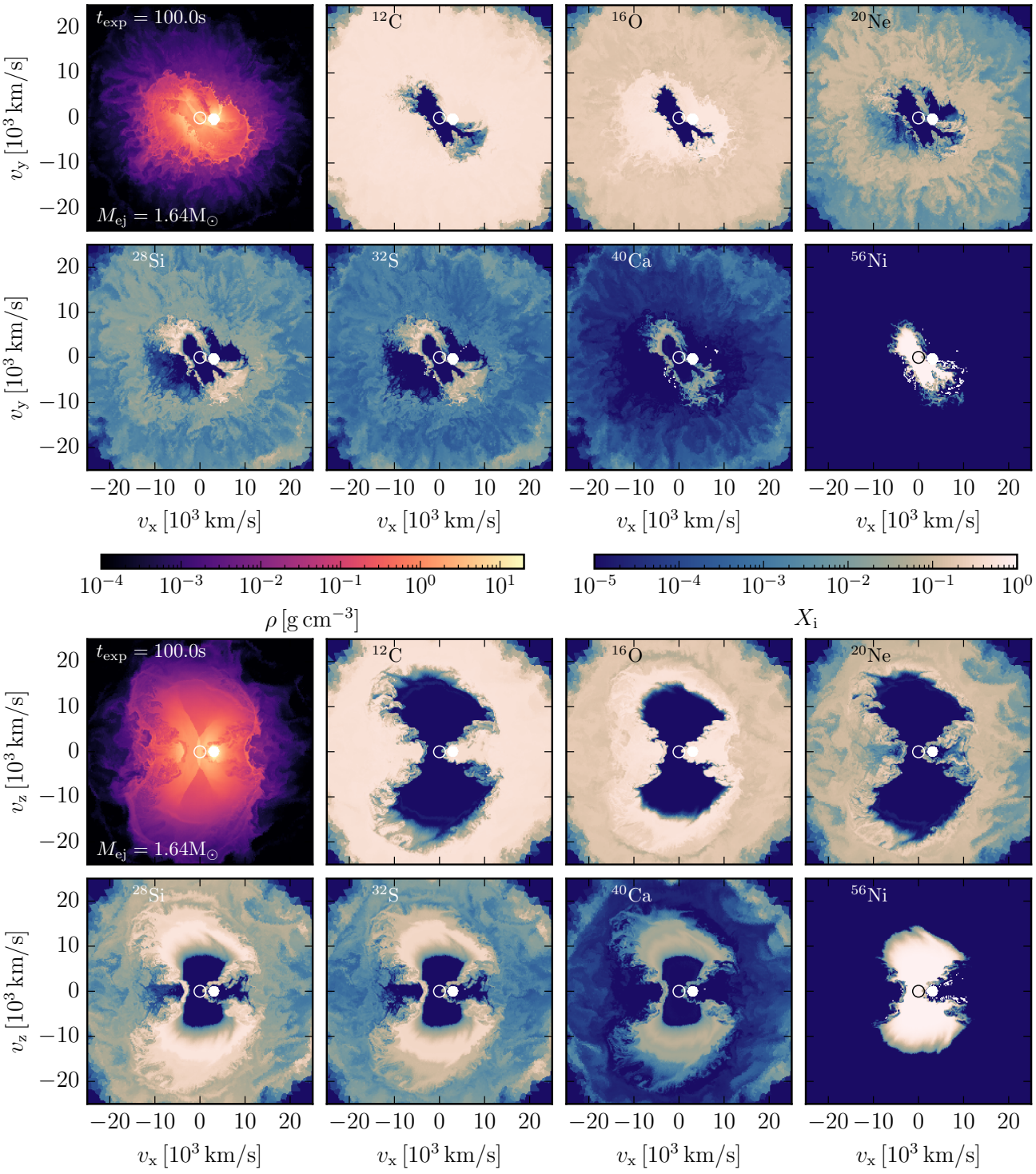

Fig. 3. Slices through the ejecta 100 s after the explosion in the plane of rotation of the binary system (top rows) and perpendicular to it (bottom rows). At this time the ejecta are fully in homologous expansion. The panels show the density in the top-left panel, and mass fractions of different isotopes are shown in the other panels. The open circle indicates the centre of the ejecta. The filled white circle appears where the material of the bound remnant is located, which has been removed here. The structures look very similar to older violent merger simulations, showing a clear global asymmetry and material originating from the secondary white dwarf close to the centre.

and partial burning is then incorporated into the central parts of the ejecta of the primary white dwarf. The density structure of the ejecta and its composition in homologous expansion 100 s after ignition are shown in Fig. 3. The ejecta contain a total mass of 1.64 $M_\odot$, and notably 0.72 $M_\odot$ of radioactive ^{56}Ni, 0.03 $M_\odot$ of stable ^{58}Ni, 0.02 $M_\odot$ of ^{40}Ca, 0.16 $M_\odot$ of ^{28}Si, 0.29 $M_\odot$ of ^{16}O, 0.03 $M_\odot$ of ^{20}Ne, and 0.19 $M_\odot$ of ^{12}C. Most of the material of the initial binary system is part of the ejecta. The total centre-of-mass velocity of the ejecta with respect to the rest frame of the original binary system is only 290 km/s.

The ejecta composition and structure is very similar to previous violent merger simulations (Pakmor et al. 2012a; Sato et al.

2015). Most of the ejecta material originating from the secondary white dwarf is unburned. However, some of its carbon has been burned to neon, which, together with unburned carbon and oxygen, is located close to the very centre of the ejecta. In particular, the burning of the secondary white dwarf still produces 0.025 $M_\odot$ of ^{20}Ne, about a third of what was produced in the old simulation in which the secondary was completely burned (Pakmor et al. 2012a). Neon in the centre of the ejecta is of particular interest because it has so far only been seen in JWST observations of nebular spectra of SN 2022pul, a 03fg-like Type Ia supernovae that has been argued to be a violent merger (Blondin et al. 2023; Kwok et al. 2024). Moreover, SN 2022pul has also been shown to have carbon in the centre of the ejecta (Liu et al. 2025), that is naturally explained by our ejecta structure. However, the detailed morphology of the central ejecta is complicated, so only future 3D radiative transfer simulations of the nebular phase (Pollin et al. 2025) of this model will be able to show if our model produces similar neon and carbon lines in the nebular spectrum as observed for SN 2022pul.

Above and below the orbital plane, the ashes of the primary white dwarf spread much further out in velocity space than in the plane of rotation. The iron group elements reach velocities above 10^4 km/s in the vertical direction. We leave detailed radiation transfer post-processing and a comparison of synthetic observables with observations and previous simulations to future work. We expect synthetic observables of our explosion to show significant line of sight variation and overall polarisation, similar to previous violent merger models (Pakmor et al. 2012a; Bulla et al. 2016).

4. Remnant

The main difference between our simulation and previous violent merger simulations is the presence of a surviving bound remnant. The remnant is the remainder of the core of the secondary white dwarf that is not disrupted from the impact of the explosion (see Fig. 2). When the secondary white dwarf is hit by the explosion of the primary white dwarf, it is already in the process of being disrupted and accelerated towards the primary white dwarf. The material that remains bound is therefore significantly faster than the orbital velocity of the binary at the time of ignition and moves with a velocity of 2800 km/s relative to the rest frame of the original binary system.

The high velocity ($\gg$2000 km/s) of the surviving star is so far a unique feature of the violent merger scenario. It arises from an initial orbital velocity of ∼2000 km/s due to the high total mass of the binary system (Shen et al. 2018) and the additional acceleration of the secondary white dwarf towards the primary white dwarf on its last orbit. In contrast, a massive binary system in which the primary white dwarf explodes via a double detonation explosion before the secondary is disrupted (Pakmor et al. 2013; Shen et al. 2018; Braudo & Soker 2024) has an upper limit on the ejection velocity of the surviving star of ≈2000 km/s. A similar maximum ejection velocity limit applies for an explosion of the primary white dwarf when the secondary is disrupted in a binary system with a much lower total mass (Glanz et al. 2025).

The high velocity of our surviving star can explain the velocities of D6-1 and D6-3, the fastest of the objects found in the original search for hypervelocity stars (Shen et al. 2018), as well as the fastest hypervelocity stars found since then (El-Badry et al. 2023). Moreover, more detailed modelling indicates masses for D6-1 and D6-3 of only 0.1 $M_\odot$−0.2 $M_\odot$ (Shen 2025), which are also fully consistent with our scenario. These low masses, however, are inconsistent with double detonation explosion scenarios where the secondary white dwarf is unscathed (Bauer et al. 2021; Pakmor et al. 2022) or only slightly distorted and stripped (Glanz et al. 2025). In those scenarios the surviving star still has a mass of 0.5 $M_\odot$ or more. We discuss the potential of the violent merger scenario to produce other very fast but likely more massive hypervelocity stars (El-Badry et al. 2023) at the end of this section.

We show slices of the bound material 1000 s after the explosion in Fig. 4. At this time, the inner part of the bound remnant out to a radius of ≈0.05 $R_\odot$ has relaxed to an essentially spherically symmetric state and does not rotate. The outer parts at larger radii are still far from spherical and feature significant radial and azimuthal velocity components. However, due to computational constraints, we cannot evolve it in AREPO until it would also be relaxed in the outer parts.

We show radial profiles of the bound remnant at 1000 s after the explosion in Fig. 5. At this time, 0.16 $M_\odot$ are bound. Roughly 0.1 $M_\odot$ of them are contained within the inner 0.05 $R_\odot$ (see lower left panel of Fig. 5) where they have already relaxed to be spherically symmetric (see Fig. 4). The additional bound mass is spread out to much larger radii, and the total bound mass is only reached at a solar radius. At these larger radii the material is significantly supported by rotation and radial motions (see upper middle panel of Fig. 5). The outermost parts appear technically unbound, though this is an artefact of the spherical averaging of the remnant that is far from spherical symmetric at these large radii. The outer parts also contain almost all of the angular momentum of the bound remnant (see lower middle panel of Fig. 5). As shown in the profile of the mean atomic weight (see lower right panel of Fig. 5) the ejecta are for the most part just made from the unburned material of the secondary white dwarf. The bound remnant consists of 0.07 $M_\odot$ of carbon and 0.09 $M_\odot$ of oxygen. Only the very outermost layers contain some of the burned ashes of the primary white dwarf, including 10^{-4} $M_\odot$ of ^{56}Ni. The bound remnant features temperatures of ≈10^7 K for most of its relaxed parts (see upper right panel of Fig. 5).

While the high velocity and low mass of the bound remnant make it a prime candidate to explain the hypervelocity stars D6-1 and D6-3 (Shen et al. 2018; Shen 2025), detailed modelling is required to fully confirm or reject this association (Bhat et al. 2025; Glanz et al. 2025). This modelling will be complicated by the significant deviation from spherical symmetry of a third of the material of the bound remnant even 1000 s after the explosion. Notably, the surviving star in the violent merger scenario might have been detected already in a SN 2020hvf, which is part of the sub-class of 03fg-like 'super-Chandrasekhar' Type Ia supernovae (Siebert et al. 2023).

It is hard to assess how robust the results are with respect to the mass of the bound remnant. It will certainly depend on the detailed timing of ignition. Significantly later ignition would likely result in no bound remnant, because the secondary white dwarf would have been fully disrupted already. Significantly earlier ignition would probably leave a more massive remnant. Significantly earlier ignition seems unlikely, because the temperature increases quickly before the time when we ignite. Significantly later ignition does not seem to be likely either, because the temperature does not increase significantly beyond the temperature of 10^9 K we chose for ignition for the next 5 s.

The choice of burning limiter will probably not have a significant effect on the mass of the bound remnant. The limiter is most important for detonations at high densities, but it makes almost no difference at the low densities at which the secondary white dwarf is partially burned. The main path to more massive bound remnant

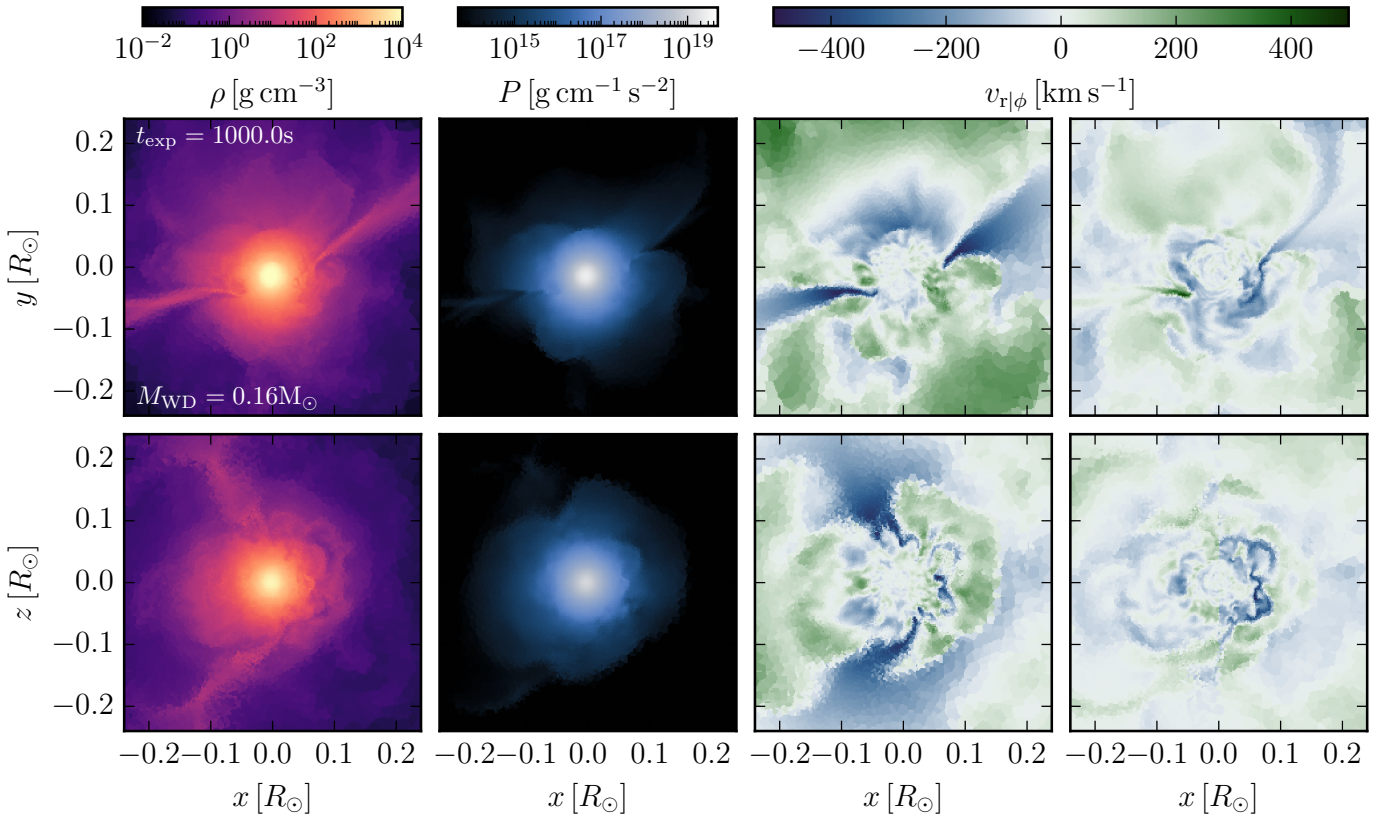

Fig. 4. Slices of density (first column), pressure (second column), radial velocity (third column), and azimuthal velocity (fourth panel) of the bound remnant 1000 s after the explosion. The top row shows slices in the plane of rotation of the initial binary system; the bottom row shows slices that are perpendicular to it. The velocities are relative to the rest frame velocity of the bound remnant. The inner part of the 0.16 $\mathrm{M}_{\odot}$ bound remnant is essentially spherical, while the outer parts are clearly not.

is probably to start from a binary system with a more massive secondary white dwarf, though this makes it even rarer.

5. Circumstellar material

The very high mass resolution of our simulation, in particular in the outer layers of the secondary white dwarf of $10^{-8}\,\mathrm{M}_{\odot}$, and the long inspiral phase prior to the explosion of more than 10 orbits allow us to have a look at the material that is ejected from the system during mass transfer before the actual explosion. Note that this phase is still significantly accelerated in our simulation by the artificial angular momentum loss term. Even in the third phase, when the additional term reduces the separation at a rate of 10 km/s, this still shrinks the binary system at least 20 times faster than in the phase before via mass transfer only without the additional term. So our results are most likely a lower limit on the pre-explosion mass loss.

For a visual impression of the circumstellar material, we show slices of density and mean atomic weight in the plane of rotation and perpendicular to it out to a distance of 0.8 $\mathrm{R}_{\odot}$ at the time of ignition in Fig. 6. We clearly see, that material has been transported out to large distances (for reference, the separation of the binary system at this time is roughly $10^{-2}\,\mathrm{R}_{\odot}$). The circumstellar material is slightly denser in the plane of rotation but extends to similarly large radii in all directions. It is dominated by unburned helium, carbon and oxygen. Its inner parts also contain heavier elements that originate from helium burning on the surface of the primary white dwarf. This material was clearly ejected later than the outermost material, so there was significant mass loss already during the accretion phase prior to any helium burning.

We quantify the properties of the circumstellar material that is unbound from the binary system at the time of ignition in Fig. 7. The top panel shows a histogram of mass in velocity space. Here, the velocity is the asymptotic velocity at infinity computed from the current velocity of each unbound cell and its local gravitational potential. The total mass of the unbound material is $3 \times 10^{-3}\,\mathrm{M}_{\odot}$, most of it at velocities below 2000 km/s with a tail to larger velocities up to 5000 km/s. This material is dominated by helium with significant mass fractions of carbon, and a smaller amount of oxygen, representing the composition of the outer layers of the secondary white dwarf. It has only minor contributions of heavier elements. The material mostly originates from the unmodified material of the outer layers of the secondary white dwarf. The material at the largest velocities has a significantly higher mass fraction of silicon and calcium; products of helium burning on the surface of the primary white dwarf. The higher velocities are a consequence of the additional extra energy release from nuclear burning, though the total mass at these large velocities is tiny.

We show the time evolution of mass transfer and mass loss from the binary system in Fig. 8. We first compute which material is unbound from the binary system, that is the mass of all cells with a positive total energy $\epsilon_{\mathrm{tot}} = \epsilon_{\mathrm{thermal}} + \epsilon_{\mathrm{kinetic}} + \epsilon_{\mathrm{potential}}$. The remaining material is bound to the binary system. We further sub-divided the bound material by computing the potential at the inner Lagrange point L1. We then count all material at a higher potential as 'fluff' that is only bound to the binary

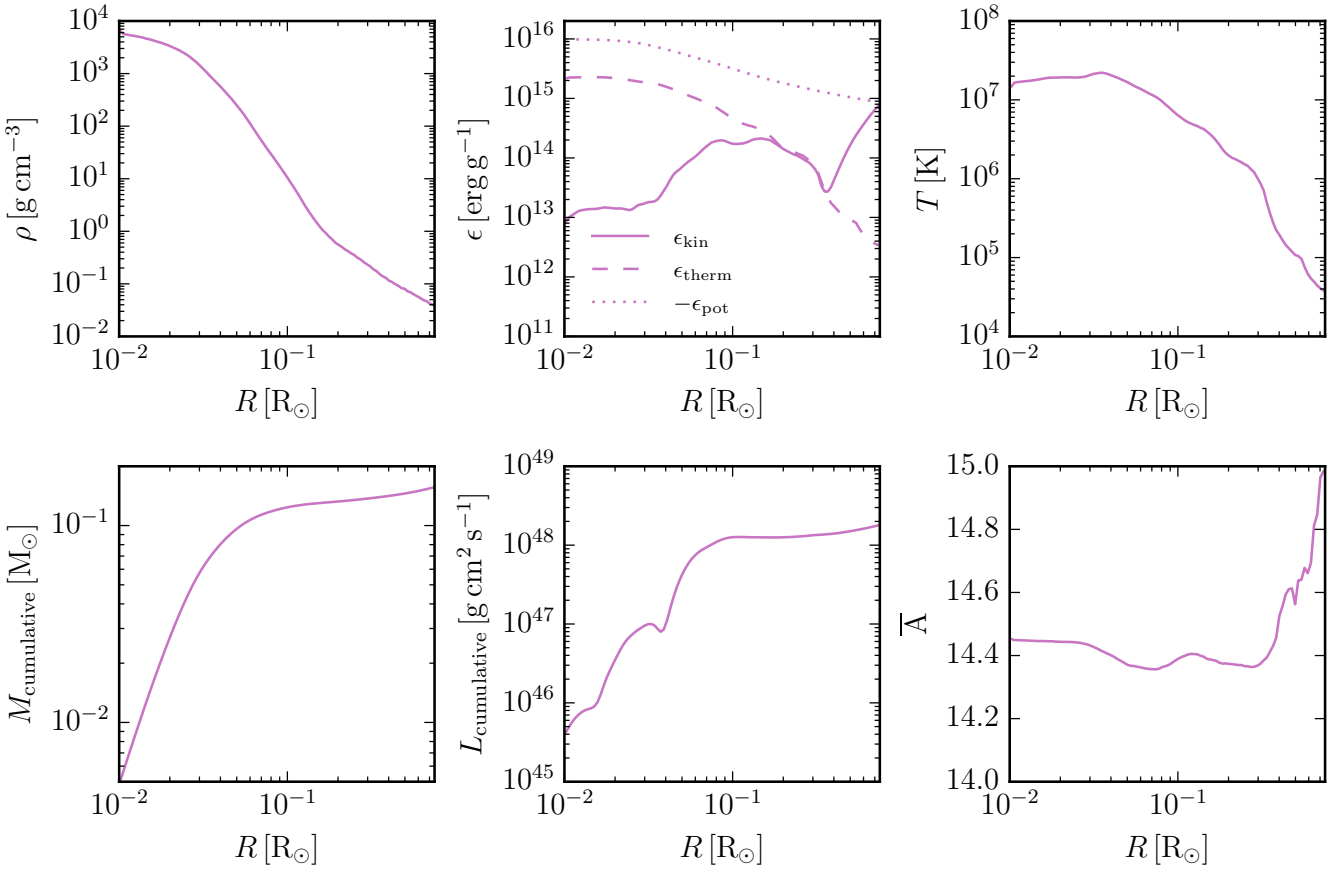

Fig. 5. Radial profiles of the bound remnant 1000 s after the explosion. The panels show, from left to right and top to bottom, profiles of density, specific energies, temperature, cumulative mass, cumulative angular momentum, and mean atomic weight. The essentially spherical part of the remnant seen in Fig. 4 extends out to a radius of about 0.04 R$_\odot$. It is essentially non-rotating and contains about half of the bound mass of the remnant. The outer parts are rotating and cold, and they contain a small amount of the heavier elements from the ashes of the explosion.

system as a whole, but cannot easily be associated with one of the individual white dwarfs. We then assign all bound material at a deeper potential than the potential at L1 to either white dwarf, depending on which side of L1 it is.

Figure 8 shows that the secondary white dwarf is losing mass at a rate of order 10^{-5} M$_\odot$/s in our simulation. Most of the material becomes bound to the primary white dwarf and increases its mass. About 10% of the material lost from the secondary white dwarf before its last orbit becomes fluff that is bound to the binary system but not obviously to one of the individual white dwarfs. Because the separation of the binary system oscillates slightly (see also Fig. 1), the potential at L1 oscillates as well. This leads to oscillations in the estimates of the mass already lost from the secondary white dwarf and the mass associated with the fluff.

A few percent of the material that is lost from the secondary white dwarf becomes unbound from the binary system. At the time of ignition, this accumulates to 3×10^{-3} M$_\odot$. This material, in particular if it reaches significant distances from the binary system when it explodes, might significantly affect observables of the supernova. We look at this as a first step to understand how much material is actually ejected during the inspiral phase and what properties it might have. Again, because of the accelerated inspiral, this is likely a lower limit on the amount of mass lost, and certainly a lower limit on the distance at which we would find this material at the time of explosion. When we compute the unbound mass ignoring its thermal energy, that is only comparing kinetic and potential energy, the unbound mass evolves similarly to Fig. 8, but is about a factor of two smaller.

The ejecta velocities and total mass are qualitatively consistent with lower resolution smoothed particle hydrodynamics simulations of mergers of two carbon-oxygen white dwarfs (Raskin & Kasen 2013). In our simulation the material is ejected over a few hundred seconds with a typical velocity of 1000 km/s. Since the inspiral in our simulation is faster by at least a factor of 20 than in reality (see Sect. 3), the inspiral phase should last correspondingly longer. The ejected material can thus reach distances of 10^{12} cm as a conservative estimate. The ejecta of the explosion, that are roughly ten times faster than the material ejected during inspiral, will reach the circumstellar material likely on the first day after explosion. The interaction between the ejecta and this material might produce a bump in the light curve at early times. The amount and properties of the circumstellar material in our simulation are roughly in the regime of the circumstellar material argued to be around the two 03fg-like Type Ia supernovae SN 2021zny (0.04 M$_\odot$ at a distance of 10^{12} cm, Dimitriadis et al. 2023) and SN 2022ilv (10^{-3} to 10^{-2} M$_\odot$ at a distance of 10^{13} cm, Srivastav et al. 2023a). In the future, we will need better modelling of the ejection of material during inspiral as well as detailed modelling of the interaction of the ejecta with the previously ejected material to understand these early-time observations.

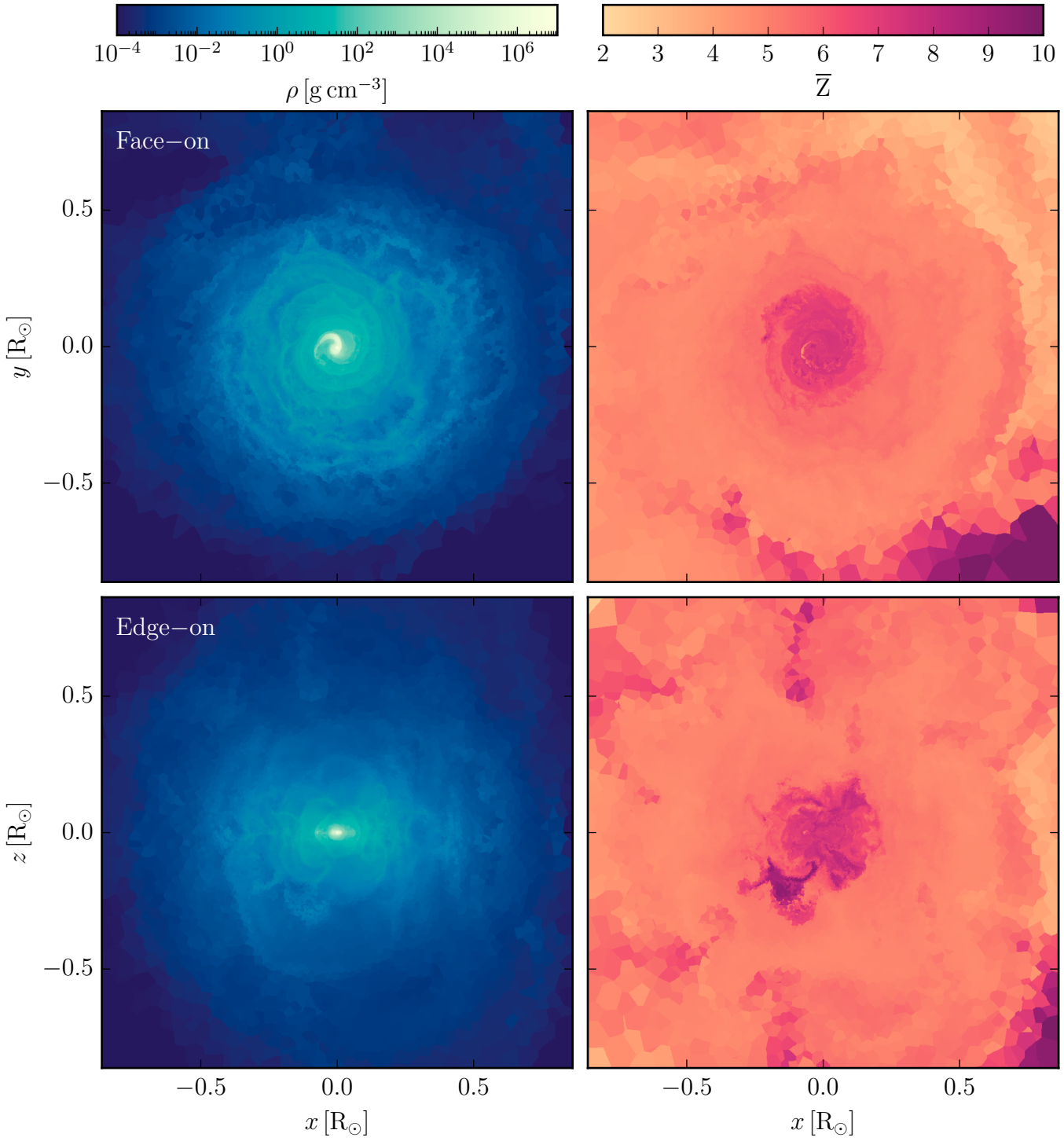

Fig. 6. Slices of density (left column) and mean charge (right column) of the whole simulation box at the time of explosion. The top row shows slices in the plane of rotation of the binary system, the bottom row shows slices perpendicular to it. There are clear outflows to large distances from the binary system even before the explosion. These outflows contain some heavier metals at various distances as a result of explosive helium burning on the surface of the primary white dwarf during the inspiral.

6. Discussion

The critical condition for a binary system of two sufficiently massive carbon-oxygen white dwarfs to explode via the violent merger scenario is that the primary white dwarf does not explode before already via the double detonation mechanism. If a double detonation ignition of the primary white dwarf is possible, it will always happen earlier, because a helium detonation ignites at much lower temperatures and densities than a carbon detonation.

In the simulation we present here a double detonation of the primary white dwarf is absent because its surface helium layer is too thin to support a helium detonation. This is the natural outcome for carbon-oxygen white dwarfs with a mass above $\gtrsim$1.0 M$_\odot$ that did not accrete additional helium after formation (Shen et al. 2024). This selection criterion on massive primary

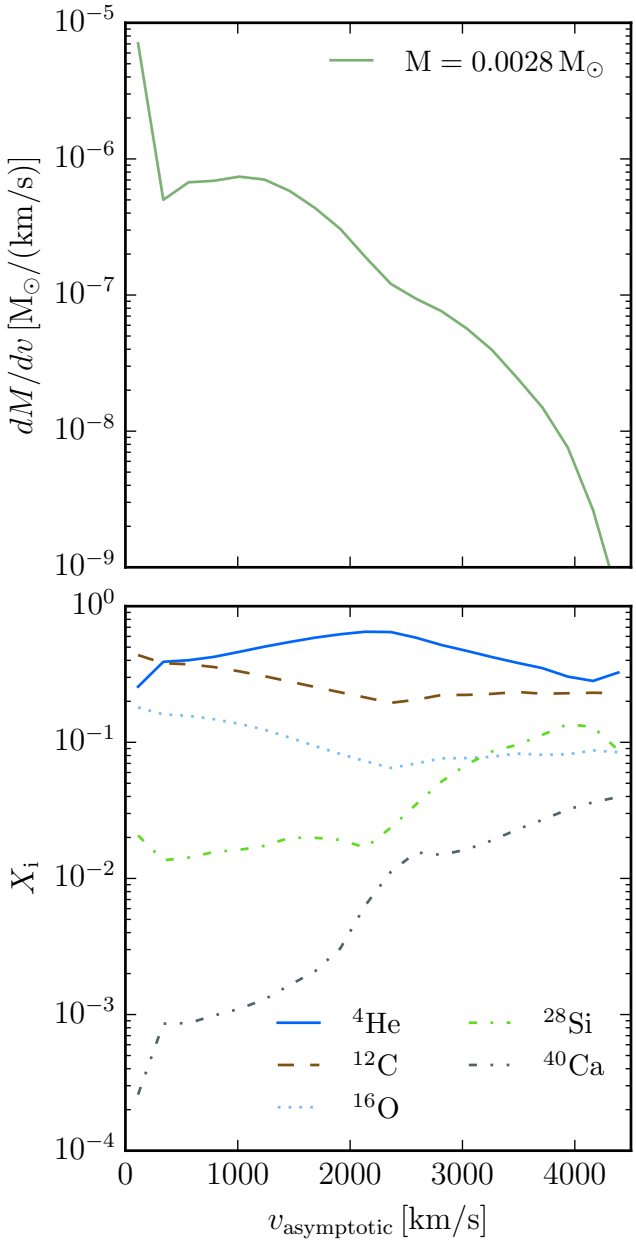

Fig. 7. Mass (top panel) and abundance (bottom panel) profiles in velocity space of the unbound material at the time of the explosion. The ejected mass has a typical velocity of 1500 km/s and consists mostly of helium, carbon, and some intermediate mass elements at the largest velocities.

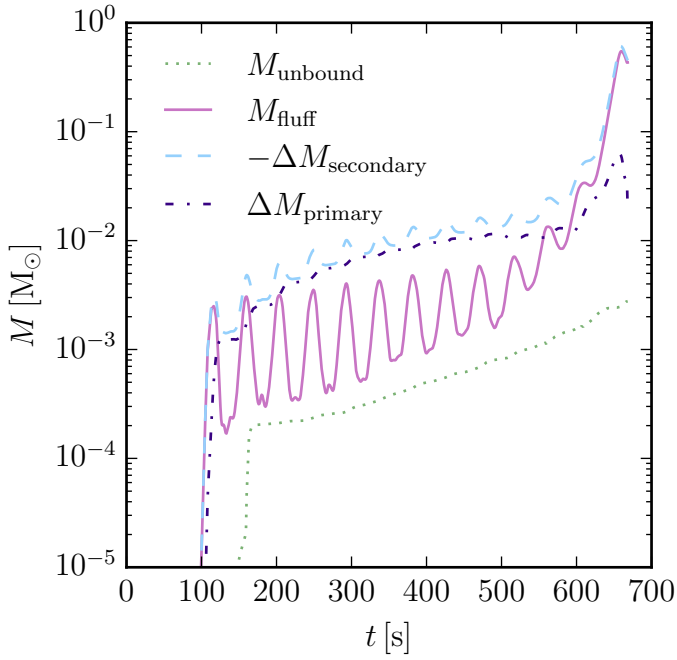

Fig. 8. Time evolution of mass transfer. We separate all mass the material lost from the secondary white dwarf ($\Delta M_{\rm secondary}$), the mass gained by the primary white dwarf ($\Delta M_{\rm primary}$), the mass only associated with the binary system as a whole ($M_{\rm fluff}$), and the unbound material $M_{\rm unbound}$. Before the explosion, about 3×10^{-3} $M_\odot$ have become unbound already.

white dwarfs helps to explain the brightness of 03fg-like ('super-Chandrasekhar') objects, that have been associated with violent mergers (Taubenberger et al. 2013a,b; Taubenberger 2017; Dimitriadis et al. 2022; Srivastav et al. 2023a; Siebert et al. 2023, 2024; Kwok et al. 2024). Moreover, our violent merger explosion can naturally explain most of the other peculiar characteristic properties of this sub-class.

In this picture, the 'bumps' in the early light curve and the unburned material in early spectra (Dimitriadis et al. 2022, 2023; Srivastav et al. 2023a; Hoogendam et al. 2024) are a direct consequence of the circumstellar material that was ejected during the last day before the explosion (see Sect. 5). This material is absent in double or quadruple detonations (Pakmor et al. 2022), because they already explode before they reach the phase of very high mass transfer rates and bursts of helium burning on the surface of the primary white dwarf that gives rise to it.

The partial burning of the secondary white dwarf naturally explains the presence of unburned material and neon close to the centre of the ejecta (see Fig. 3), that is required to explain at least some nebular spectra of 03fg-like objects (Taubenberger et al. 2019; Dimitriadis et al. 2023; Siebert et al. 2024; Kwok et al. 2024).

The low ejecta luminosities in some objects (see, for example Taubenberger et al. 2011) can in principle be explained by line of sight effects (see Fig. 3 for lines of sight close to the initial plane of the binary system). These line of sight effects might also be a reason for the additional luminosity at early times. Another contribution could come from interaction with circumstellar material. However, to be relevant, this would likely require a substantial fraction of the original mass of the secondary white dwarf to have ended up in the circumstellar material (Noebauer et al. 2016). Lastly, a wind from the surviving bound object in the centre of the ejecta that interacts with the inner ejecta when they are still optically thick in the centre could also contribute extra luminosity at early times (Shen & Schwab 2017). More work is clearly needed to really understand the source of the extra luminosity of 03fg-like objects at early times.

Violent mergers have also been associated with 02es-like objects, a sub-class of sub-luminous Type Ia supernovae (Maguire et al. 2011; Kromer et al. 2013b; Srivastav et al. 2023b; Hoogendam et al. 2024). Because they are sub-luminous, these objects cannot possibly arise from violent merger explosions with massive primary white dwarfs. Despite there being very good agreement between synthetic observables of violent mergers of lower mass carbon-oxygen white dwarf binaries with observables of 02es-like objects (Kromer et al. 2013b), it is not obvious how such systems can avoid exploding via double

detonation explosions if the helium shell on the primary white dwarf is included.

We speculate that binary systems of almost equal mass carbon-oxygen white dwarfs might also explode as violent mergers, rather than via a double detonation explosion. In this case the double detonation might be avoided because the primary white dwarf and in particular its helium shell is already distorted before the secondary white dwarf overfills its Roche lobe sufficiently to drive a dense enough accretion stream towards the primary white dwarf to ignite it. Such a scenario would bring the violent merger scenario back to its roots where it was introduced for mergers of almost equal mass white dwarfs (Pakmor et al. 2010, 2011; Kromer et al. 2013a).

In this picture, equal mass violent mergers would also be preceded by a characteristic phase in which the two Roche-lobe filling white dwarfs interact, but do not merge yet. In this phase they possibly burn helium-rich material locally, and likely eject significant amounts of material just prior to the explosion to create an envelope of circumstellar material, as seen for 02es-like objects (Hoogendam et al. 2024). The large ejecta mass of the explosion (significantly above the Chandrasekhar-mass) naturally explains the much broader light curves compared to normal sub-luminous Type Ia supernovae (Maguire et al. 2011; Ganeshalingam et al. 2012; Kromer et al. 2013a, 2016). Finally, equal mass violent mergers could also naturally explain the presence of oxygen in the centre of the ejecta seen in nebular spectra of at least some 02es-like objects (Kromer et al. 2013a). It remains to be seen if equal mass violent mergers can leave bound remnants behind, or if those are an outcome of massive violent mergers only.

The equal mass violent merger scenario will probably need a primary white dwarf with a mass above $\gtrsim 0.8\,M_\odot$ to produce an observable supernova (Ruiter et al. 2013; Shen et al. 2018). Population synthesis studies indicate that most merging binary systems of two carbon-oxygen white dwarfs have a secondary white dwarf with a mass around $0.7\,M_\odot$ (Liu et al. 2018). The equal mass violent merger scenario predicts that there exists a continuum in brightness of 02es-like objects extending all the way up to 03fg-like objects. Objects at the bright end of 02es-like Type Ia supernovae will be very rare though, but possibly detectable with LSST.

Both sub-classes that have been associated with violent mergers (03fg-like Type Ia supernovae and 02es-like Type Ia supernovae) account for approximately one percent of the Type Ia supernova rate (Dimitriadis et al. 2025). This rate roughly matches the number of fast (>2000 km/s) hypervelocity stars (Shen et al. 2018; El-Badry et al. 2023; Shen 2025). Our simulation is the first to plausibly explain the two extreme hypervelocity stars D6-1 and D6-3 (Shen et al. 2018) that are not only very fast, but also likely of low mass (Shen 2025). This combination is essentially impossible to reach in double detonation explosions, where the orbital velocity at explosion and therefore also the ejection velocity of the surviving star increase with the total mass of the system. Interestingly, D6-2, which only moving with 1000 km/s, is much too slow to be explained by the violent merger scenario, but seems to have a similar (very low) mass (Shen 2025). It remains to be shown if violent mergers can also explain the hotter, likely slightly more massive, but also very fast hypervelocity stars (El-Badry et al. 2023; Bhat et al. 2025; Glanz et al. 2025).

The rarity of surviving hypervelocity stars and the small contribution of violent mergers to the total Type Ia supernova rate are also consistent with the absence of surviving bound objects in nearby supernova remnants (Schaefer & Pagnotta 2012; González Hernández et al. 2012; Kerzendorf et al. 2018). Note that even though violent mergers seems to naturally have circumstellar material at the time of explosion, the amount of circumstellar material is likely too low to hide a bound object in a young remnant.

If 03fg-like Type Ia supernovae are indeed violent mergers with massive ($M_{\rm primary} \gtrsim 1.1\,M_\odot$) primary white dwarfs, they are almost certainly the tail of primary white dwarfs with the highest masses of a distribution of merging carbon-oxygen white dwarf binaries (Ruiter et al. 2013; Liu et al. 2018). Since they contribute ≈1% to the total Type Ia supernova rate, there will be a large population of merging double white dwarf systems with primary white dwarfs of ($M_{\rm primary} < 1.1\,M_\odot$. Most of these primaries will have a more massive helium shell, likely enough to support ignition via the double detonation scenario (Shen et al. 2024). Explosions from these systems will be at least ten times more frequent than violent mergers, because mergers of double white dwarf systems with lower mass primary white dwarfs are much more common (Liu et al. 2018) and still produce a sufficient amount of radioactive nickel to produce a type Ia supernova (Ruiter et al. 2013). This large population of type Ia supernovae can, by number, only really be explained with normal Type Ia supernovae. They likely explode by igniting the primary white dwarf via double detonation. Usually both white dwarfs will then have to explode in the quadruple detonation scenario (Tanikawa et al. 2019; Pakmor et al. 2022) because only a few percent of the Type Ia supernovae leave a surviving star behind (Shen 2025). More simulations and detailed modelling of quadruple explosions and their observables is needed to understand if these quadruple detonations can fully explain normal Type Ia supernovae (Pakmor et al. 2022; Pollin et al. 2024, 2025; Boos et al. 2025).

7. Summary and outlook

We have presented and analysed a simulation of a binary system of two carbon-oxygen white dwarfs with the moving-mesh code AREPO that follows the inspiral and explosion via the violent merger scenario. In contrast to previous simulations, the improved numerical resolution and more accurate treatment of the detonation leaves a bound low-mass ($0.16\,M_\odot$), fast moving (2800 km/s) star behind.

We discussed the inspiral, the explosion, and the ejecta structure in Sect. 3, and we found them to be very similar to previous simulations of violent mergers. In particular the ejecta are still highly asymmetric and contain carbon, oxygen, and neon close to the centre. We then looked in detail at the properties of the bound remnant in Sect. 4 and argued that it is likely consistent with the observed extreme hypervelocity stars D6-1 and D6-3 and can explain their large velocities as well as the low mass inferred for them.

In Sect. 5 we analysed the material ejected prior to the explosion that creates a circumstellar envelope. We showed that it contains a mass of at least $5 \times 10^{-3}\,M_\odot$ of mostly unburned material from the outer layers of the secondary white dwarf, with typical velocities of 1000 km/s and up to 5000 km/s. This ejected mass almost certainly only represents a lower limit because we employed an accelerated inspiral and completely neglected the earlier phase of mass transfer at much lower mass transfer rates that precede the phase of the evolution of the binary system when we started our simulation.

Most importantly, as we discussed in Sect. 6, violent mergers are not only the most likely (and so far only plausible) explanation for the origin of the hypervelocity stars D6-1 and D6-3, they also explain (at least qualitatively) most of the characteristic

properties of the Type Ia supernova sub-class of 'super-Chandrasekhar' or 03fg-like objects. We speculated that equal mass binaries of lower-mass carbon-oxygen white dwarfs could also avoid a double detonation explosion and instead explode as violent mergers. These explosions might explain sub-luminous 02es-like objects. We then argued that if the association of violent mergers with 03fg-like Type Ia supernovae holds and violent mergers are the result of the tail of the distribution of mergers of carbon-oxygen white dwarf binaries with the most massive primary white dwarfs, there has to be a much larger population of mergers with (at least slightly) lower-mass primary white dwarfs that can essentially only lead to normal Type Ia supernovae.

There are several straightforward next steps to test and confirm our results and better understand their implications. First, the long-term evolution of the surviving white dwarf needs to be properly modelled in order to understand how well it really matches D6-1 and D6-3. We will do so in a companion paper (Bhat et al., in prep.). Moreover, detailed 3D radiative transfer simulations of the ejecta need to be run, ideally including polarisation, to understand if the observables of our new simulations still match previous results on early time observables (Pakmor et al. 2012a; Bulla et al. 2016) and late time observables (Blondin et al. 2023; Kwok et al. 2024). Better modelling and understanding of the impact of circumstellar material from pre-explosion mass loss on observables is needed as well as confirmation that they can explain the early 'bumps' observed for 03fg-like and 02es-like objects (Hoogendam et al. 2024). Whether mass mergers of lower mass carbon-oxygen white dwarfs lead to violent mergers even if their helium shells are included also needs to be tested. Then the specific conditions that give rise to a violent merger rather than a double detonation explosion of the primary (and possibly secondary) white dwarf needs to be determined more precisely. Finally, better study of quadruple detonations are needed to confirm that they are fully consistent with normal Type Ia supernovae.

Acknowledgements. The authors gratefully acknowledge the Gauss Centre for Supercomputing e.V. (www.gauss-centre.eu) for funding this project by providing computing time on the GCS Supercomputer SuperMUC-NG at Leibniz Supercomputing Centre (www.lrz.de) via the project pn76fu. KJS is supported by NASA through the Astrophysics Theory Program (80NSSC20K0544) and by NASA/ESA Hubble Space Telescope program No. 17441. KM acknowledges funding from Horizon Europe ERC grant no. 101125877. FPC would like to acknowledge support from the UK Science and Technology Facilities Council (STFC, grant number ST/X00094X/1). CEC is funded by the European Union's Horizon Europe research and innovation programme under the Marie Skłodowska-Curie grant agreement No. 101152610. LAK is supported by NASA through a Hubble Fellowship grant No. HF2-51579.001-A awarded by the Space Telescope Science Institute (STScI), which is operated by the Association of Universities for Research in Astronomy, Inc., for NASA, under contract NAS5-26555. Work by EB was performed under the auspices of the U.S. Department of Energy by Lawrence Livermore National Laboratory under Contract DE-AC52-07NA27344. A.B. was supported by the Deutsche Forschungsgemeinschaft (DFG) through grant GE2506/18-1. The work of FKR is supported by the Klaus Tschira Foundation, by the Deutsche Forschungsgemeinschaft (DFG, German Research Foundation) – RO 3676/7-1, project number 537700965, and by the European Union (ERC, ExCEED, project number 101096243). Views and opinions expressed are, however, those of the authors only and do not necessarily reflect those of the European Union or the European Research Council Executive Agency. Neither the European Union nor the granting authority can be held responsible for them.

References

Bauer, E. B., Chandra, V., Shen, K. J., & Hermes, J. J. 2021, ApJ, 923, L34
Bhat, A., Bauer, E. B., Pakmor, R., et al. 2025, A&A, 693, A114
Blondin, S., Dessart, L., Hillier, D. J., Ramsbottom, C. A., & Storey, P. J. 2023, A&A, 678, A170
Boos, S. J., Dessart, L., Townsley, D. M., & Shen, K. J. 2025, ApJ, 987, 54
Braudo, J., & Soker, N. 2024, Open J. Astrophys., 7, 7
Bulla, M., Sim, S. A., Pakmor, R., et al. 2016, MNRAS, 455, 1060
Burmester, U. P., Ferrario, L., Pakmor, R., et al. 2023, MNRAS, 523, 527
Cyburt, R. H., Amthor, A. M., Ferguson, R., et al. 2010, ApJS, 189, 240
Dimitriadis, G., Foley, R. J., Arendse, N., et al. 2022, ApJ, 927, 78
Dimitriadis, G., Maguire, K., Karambelkar, V. R., et al. 2023, MNRAS, 521, 1162
Dimitriadis, G., Burgaz, U., Deckers, M., et al. 2025, A&A, 694, A10
Dunkley, S. D., Sharpe, G. J., & Falle, S. A. E. G. 2013, MNRAS, 431, 3429
El-Badry, K., Shen, K. J., Chandra, V., et al. 2023, Open J. Astrophys., 6, 28
Fryxell, B., Müller, E., & Arnett, D. 1989, in Nuclear Astrophysics, eds. M. Lozano, M. I. Gallardo, & J. M. Arias, 100
Ganeshalingam, M., Li, W., Filippenko, A. V., et al. 2012, ApJ, 751, 142
Glanz, H., Perets, H. B., Bhat, A., & Pakmor, R. 2025, Nat. Astron., 9, 1523
González Hernández, J. I., Ruiz-Lapuente, P., Tabernero, H. M., et al. 2012, Nature, 489, 533
Guillochon, J., Dan, M., Ramirez-Ruiz, E., & Rosswog, S. 2010, ApJ, 709, L64
Hoogendam, W. B., Shappee, B. J., Brown, P. J., et al. 2024, ApJ, 966, 139
Kerzendorf, W. E., Strampelli, G., Shen, K. J., et al. 2018, MNRAS, 479, 192
Kromer, M., Pakmor, R., Taubenberger, S., et al. 2013a, ApJ, 778, L18
Kromer, M., Fink, M., Stanishev, V., et al. 2013b, MNRAS, 429, 2287
Kromer, M., Fremling, C., Pakmor, R., et al. 2016, MNRAS, 459, 4428
Kushnir, D., & Katz, B. 2020, MNRAS, 493, 5413
Kwok, L. A., Siebert, M. R., Johansson, J., et al. 2024, ApJ, 966, 135
Liu, D., Wang, B., & Han, Z. 2018, MNRAS, 473, 5352
Liu, Z.-W., Röpke, F. K., & Han, Z. 2023, RAA, 23, 082001
Liu, J., Wang, X., Yang, Y., et al. 2025, ApJ, 982, L18
Maguire, K., Sullivan, M., Thomas, R. C., et al. 2011, MNRAS, 418, 747
Noebauer, U. M., Taubenberger, S., Blinnikov, S., Sorokina, E., & Hillebrandt, W. 2016, MNRAS, 463, 2972
Ohlmann, S. T., Röpke, F. K., Pakmor, R., & Springel, V. 2017, A&A, 599, A5
Pakmor, R., Kromer, M., Röpke, F. K., et al. 2010, Nature, 463, 61
Pakmor, R., Hachinger, S., Röpke, F. K., & Hillebrandt, W. 2011, A&A, 528, A117
Pakmor, R., Edelmann, P., Röpke, F. K., & Hillebrandt, W. 2012a, MNRAS, 424, 2222
Pakmor, R., Kromer, M., Taubenberger, S., et al. 2012b, ApJ, 747, L10
Pakmor, R., Kromer, M., Taubenberger, S., & Springel, V. 2013, ApJ, 770, L8
Pakmor, R., Springel, V., Bauer, A., et al. 2016, MNRAS, 455, 1134
Pakmor, R., Zenati, Y., Perets, H. B., & Toonen, S. 2021, MNRAS, 503, 4734
Pakmor, R., Callan, F. P., Collins, C. E., et al. 2022, MNRAS, 517, 5260
Paxton, B., Bildsten, L., Dotter, A., et al. 2011, ApJS, 192, 3
Pollin, J. M., Sim, S. A., Pakmor, R., et al. 2024, MNRAS, 533, 3036
Pollin, J. M., Sim, S. A., Shingles, L. J., et al. 2025, MNRAS, submitted [arXiv:2507.05000]
Raskin, C., & Kasen, D. 2013, ApJ, 772, 1
Ruiter, A. J., & Seitenzahl, I. R. 2025, A&ARv, 33, 1
Ruiter, A. J., Sim, S. A., Pakmor, R., et al. 2013, MNRAS, 429, 1425
Saio, H., & Nomoto, K. 1985, A&A, 150, L21
Sato, Y., Nakasato, N., Tanikawa, A., et al. 2015, ApJ, 807, 105
Sato, Y., Nakasato, N., Tanikawa, A., et al. 2016, ApJ, 821, 67
Schaefer, B. E., & Pagnotta, A. 2012, Nature, 481, 164
Schwab, J. 2021, ApJ, 906, 53
Schwab, J., Shen, K. J., Quataert, E., Dan, M., & Rosswog, S. 2012, MNRAS, 427, 190
Seitenzahl, I. R., Meakin, C. A., Townsley, D. M., Lamb, D. Q., & Truran, J. W. 2009, ApJ, 696, 515
Shen, K. J. 2025, ApJ, 982, 6
Shen, K. J., & Moore, K. 2014, ApJ, 797, 46
Shen, K. J., & Schwab, J. 2017, ApJ, 834, 180
Shen, K. J., Bildsten, L., Kasen, D., & Quataert, E. 2012, ApJ, 748, 35
Shen, K. J., Kasen, D., Miles, B. J., & Townsley, D. M. 2018, ApJ, 854, 52
Shen, K. J., Blouin, S., & Breivik, K. 2023, ApJ, 955, L33
Shen, K. J., Boos, S. J., & Townsley, D. M. 2024, ApJ, 975, 127
Siebert, M. R., Foley, R. J., Zenati, Y., et al. 2023, ApJ, 958, 173
Siebert, M. R., Kwok, L. A., Johansson, J., et al. 2024, ApJ, 960, 88
Springel, V. 2005, MNRAS, 364, 1105
Springel, V. 2010, MNRAS, 401, 791
Srivastav, S., Smartt, S. J., Huber, M. E., et al. 2023a, ApJ, 943, L20
Srivastav, S., Moore, T., Nicholl, M., et al. 2023b, ApJ, 956, L34
Tanikawa, A., Nomoto, K., Nakasato, N., & Maeda, K. 2019, ApJ, 885, 103
Taubenberger, S. 2017, in Handbook of Supernovae, eds. A. W. Alsabti, & P. Murdin, 317
Taubenberger, S., Benetti, S., Childress, M., et al. 2011, MNRAS, 412, 2735
Taubenberger, S., Kromer, M., Pakmor, R., et al. 2013a, ApJ, 775, L43
Taubenberger, S., Kromer, M., Hachinger, S., et al. 2013b, MNRAS, 432, 3117
Taubenberger, S., Floers, A., Vogl, C., et al. 2019, MNRAS, 488, 5473
Timmes, F. X., & Swesty, F. D. 2000, ApJS, 126, 501
Weinberger, R., Springel, V., & Pakmor, R. 2020, ApJS, 248, 32